J. Fluid Mech. (2004), *vol.* 502, *pp.* 127–152.
DOI: 10.1017/S0022112003007675 Printed in the United Kingdom

Evaluation of scaling laws derived from Lie group symmetry methods in zero-pressure-gradient turbulent boundary layers

By BJÖRN LINDGREN[1], JENS M. ÖSTERLUND[2] AND ARNE V. JOHANSSON[1]

[1]Department of Mechanics, KTH, SE-100 44 Stockholm, Sweden

[2]Swedish Defence Research Agency, Aeronautics FFA, SE-172 90 Stockholm, Sweden

(Received 6 November 2002 and in revised form 6 October 2003)

New scaling laws for turbulent boundary layers recently derived (see Oberlack 2000) using Lie group symmetry methods have been tested against experimental data from the KTH database for zero-pressure-gradient turbulent boundary layers. The most significant new law predicts an exponential variation of the mean velocity defect in the outer (wake) region. It was shown to fit the experimental data very well over a large part of the boundary layer, from the outer part of the overlap region to about half the boundary layer thickness (δ_{99}). In the outermost part of the boundary layer the velocity defect falls more rapidly than predicted by the exponential law. This can partly be attributed to intermittency in that region but the main cause stems from non-parallel effects that are not accounted for in the derivation of the exponential law. The two-point correlation function behaviour in the outer region, where an exponential velocity defect law is observed, was found to be very different from that derived under the assumption of parallel flow. It is found to be plausible that this indeed can be attributed to non-parallel effects. A small modification of the innermost part of the log-layer in the form of an additive constant within the log-function is predicted by the Lie group symmetry method. A qualitative agreement with such a behaviour just below the overlap region was found. The derived scaling law behaviour in the overlap region for the two-point correlation functions was also verified by the experimental data.

1. Introduction and theoretical considerations

Scaling issues in turbulent wall-bounded shear flows have been a topic of much debate since the two-layer hypothesis was introduced by Millikan and von Kármán (see von Kármán 1930 and Millikan 1938). In this paper the idea of using continuous transformation group (Lie group) symmetries to identify scaling laws in different regions of zero-pressure-gradient turbulent boundary layer flow is evaluated using data from experiments and direct numerical simulations. The use of Lie group symmetries is a very general tool for identification of possible similarity solutions to the flow equations. The scaling laws tested here have been obtained by Oberlack (1999, 2000, 2001). The description of the Lie group algebra here follows that of Oberlack (2002). In the recent book by Cantwell (2002) Lie group symmetry methods for fluid flows are described in detail, and free turbulent shear flows are given particular attention.

The approach of obtaining scaling laws by means of Lie group symmetry methods offers a high degree of generality and allows study of the influence of, for example, boundary conditions in a systematic manner. An additional important feature is that similarity-type solutions found by means of symmetry methods are guaranteed to be admitted by the underlying equations.

In recent years there has been a large number of papers published on the issue of the functional form of the mean velocity distribution in the overlap region between the inner (near-wall) and outer regions. Alternatives to the traditional log-law have been proposed by for example Barenblatt (1993), George & Castillo (1997) and others. Österlund, Johansson & Nagib (2000*a*) and Österlund *et al.* (2000*b*) tested these competing theories using highly accurate measurements in high-Reynolds-number turbulent boundary layer flow with zero pressure gradient and found that the classical theory still seemed to give the most accurate representation of the data.

In the two-layer description of wall-bounded shear flows the mean velocity is given by

$$\overline{u}_1^+ \equiv \frac{\overline{u}_1}{u_\tau} = f(x_2^+) \quad \text{in the inner region,} \tag{1.1}$$

$$\frac{\overline{u}_\infty - \overline{u}_1}{u_\tau} = F(\eta) \quad \text{in the outer region,} \tag{1.2}$$

where $\overline{u}_1$ is the streamwise velocity, u_τ is the friction velocity, $\overline{u}_1^+ = \overline{u}_1/u_\tau$, $\overline{u}_\infty$ is the free-stream velocity, x_2 is the wall-normal coordinate, $x_2^+ = x_2 u_\tau/\nu$, and $\eta = x_2/\Delta$ where Δ is a measure of the boundary layer thickness.

The classical description of the overlap region can be given as

$$\overline{u}_1^+ = \frac{1}{\varkappa}\ln x_2^+ + B \tag{1.3}$$

or equivalently

$$\frac{\overline{u}_\infty - \overline{u}_1}{u_\tau} = -\frac{1}{\varkappa}\ln\eta + C. \tag{1.4}$$

A short description of the Lie group symmetry method is given in Appendix A. This description essentially follows that of Oberlack (2002). There we consider flows (without system rotation) that depend only on one independent coordinate, the wall-normal distance x_2. The inviscid dynamics are studied by considering the equation for the steady two-point correlation tensor,

$$R_{ij}(\boldsymbol{x}, \boldsymbol{r}) = \overline{u_i'(\boldsymbol{x}, t)u_j'(\boldsymbol{x}+\boldsymbol{r}, t)}, \tag{1.5}$$

for positions, $\boldsymbol{x}$, where the influence from viscous stresses etc. is negligible, and for separations, $\boldsymbol{r}$, large enough to be associated with length scales that are negligibly influenced by viscosity.

The approach of studying the evolution equation for the two-point correlation function is particularly interesting since it offers the possibility of studying essentially inviscid dynamics. Under these specified conditions the evolution equation for R_{ij} can readily be derived from the Euler equations, giving the inviscid equation for the fluctuating part of the velocity. The resulting evolution equation for R_{ij} inherits the symmetries from the Euler equations, which yields an interesting possibility for new insights into turbulence dynamics through the transferred Lie group symmetries.

Under the assumption of parallel flow, where the mean velocity can be written as $\overline{u}_i = \overline{u}_1(x_2)\delta_{i1}$, the admitted symmetries can (see Appendix A) be described by an

equation of characteristics in the following manner:

$$\frac{\mathrm{d}x_2}{k_{s_1}x_2 + k_{x_2}} = \frac{\mathrm{d}r_{[k]}}{k_{s_1}r_{[k]}} = \frac{\mathrm{d}\overline{u}_1}{(k_{s_1} - k_{s_2})\overline{u}_1 + k_{\overline{u}_1}} = \frac{\mathrm{d}R_{[ij]}}{2(k_{s_1} - k_{s_2})R_{[ij]}} = \cdots, \tag{1.6}$$

where square brackets mean that summation over repeated indices should not be made. It can also be seen as a four-parameter symmetry group, where the four parameters are $k_{s_1}, k_{x_2}, k_{s_2}, k_{\overline{u}_1}$. We can, for instance, see from equation (1.6) that the first two are associated with a scaling and translation transformation of the wall distance. By specification of the values of the two scaling symmetry constants, k_{s_1} and k_{s_2}, scaling laws for different planar shear flows can be obtained.

1.1. *Plane wall-bounded shear flows*

Sufficiently close to the solid boundary in wall-bounded flows such as a zero-pressure-gradient boundary layer or channel flow, we have a region of constant total shear stress. This can be described by

$$u_\tau^2 = \nu\frac{\partial\overline{u}_1}{\partial x_2} - \overline{u_1'u_2'}. \tag{1.7}$$

In the region of strong viscous influence it can be shown that we must have $k_{s_2} = 2k_{s_1}$ (and $k_{x_2} = k_{\overline{u}_1} = 0$ near a boundary) and we simply retrieve the linear profile near the wall. Obviously, the full set of symmetries described by equation (1.6) can only apply in regions where viscous stresses are negligible.

1.2. *The overlap region*

We note that in the region where equation (1.7) is valid, the friction velocity, u_τ, can be seen as an external parameter or boundary condition which inhibits the free scaling of the streamwise velocity, $\overline{u}_1$. Let us now consider a region where equation (1.7) is valid, but restrict our attention to the part sufficiently far from the wall such that the viscous influence is negligible. Since no scaling of the streamwise velocity is admitted, we see from equation (1.6) that $k_{s_1} - k_{s_2}$ must be equal to zero, i.e. $k_{s_1} = k_{s_2}$. Inserting this into equation (1.6) and integrating we find the following expression for the streamwise velocity:

$$\overline{u}_1 = \frac{k_{\overline{u}_1}}{k_{s_1}}\ln\left(x_2 + \frac{k_{x_2}}{k_{s_1}}\right) + B'. \tag{1.8}$$

In this form, which was derived by Oberlack (see e.g. Oberlack 2001) we recognize the classical log-law but with an extra constant $A = k_{x_2}/k_{s_1}$ inside the logarithm. We also recognize the Kármán constant $\varkappa = k_{s_1}/k_{\overline{u}_1}$. In viscous scaling equation (1.8) can be written as

$$\overline{u}_1^+ = \frac{1}{\varkappa}\ln(x_2^+ + A^+) + B. \tag{1.9}$$

To understand the influence of the new constant A^+ we make a series expansion with respect to x_2^+,

$$\overline{u}_1^+ = \frac{1}{\varkappa}\ln x_2^+ + B + \frac{A^+}{\varkappa}\frac{1}{x_2^+} + \text{h.o.t.} \tag{1.10}$$

Hence, the extra term associated with the new constant A can be regarded as a small, higher-order, term in the overlap. The fixed location of the wall implies that this parameter must be of negligible influence in the overlap region. Hence, A^+ must be small in comparison with the x_2^+-values in the region where the symmetry should

be valid (where the viscous influence is negligible). In the results section we will investigate whether an influence from such a term can be detected just below the overlap region.

Afzal & Yajnik (1973) have proposed similar forms of the log-law using a series expansion. Buschmann & Gad-el-Hak (2002) have also investigated this form, and Wosnik, Castillo & George (2000) studied it for the pipe flow case.

When free scaling of the mean velocity, $\overline{u}_1$, is inhibited we readily see from the characteristic equation (1.6) that (see also Oberlack 2001)

$$R_{ij} = \tilde{R}_{ij}(\boldsymbol{r}/x_2). \tag{1.11}$$

1.3. *The outer region*

In the outer region of the flow we consider wall distances of the order of the outer lengthscale, i.e. a scale that is of the order of the boundary layer thickness. In this region the flow is, hence, influenced by the outer geometrical restriction. This acts as a boundary condition and is thereby a symmetry-breaking condition that prohibits a free scaling of the wall-normal coordinate. In the symmetry group described by equation (1.6) we must, hence, put $k_{s_1} = 0$, which implies that

$$\frac{\mathrm{d}\overline{u}_1}{\mathrm{d}x_2} = -\frac{k_{s_2}}{k_{x_2}}\overline{u}_1 + \frac{k_{\overline{u}_1}}{k_{x_2}}. \tag{1.12}$$

Integration gives

$$\overline{u}_1 = C_{exp}\exp\left(-\frac{k_{s_2}}{k_{x_2}}x_2\right) + \frac{k_{\overline{u}_1}}{k_{s_2}}. \tag{1.13}$$

This velocity law derived by Oberlack (2001) is the first that has been obtained from first principles for (parts of) the outer region. This is a remarkable finding and will be tested against experimental data in § 2.

If k_{s_2}/k_{x_2} is positive we find that $\overline{u}_1$ approaches a constant value as $x_2 \to \infty$. This is compatible with a boundary-layer situation in a semi-infinite domain. In particular, we will consider zero-pressure-gradient turbulent boundary layers. The free-stream boundary condition implies that

$$\frac{k_{\overline{u}_1}}{k_{s_2}} = \overline{u}_\infty. \tag{1.14}$$

The outer region is sometimes referred to as the wake region (see Coles 1956) or velocity defect region. There have been some successful efforts to find a universal expression for the wake region, see e.g. Schultz-Grunow (1940) and Lewkowicz (1982). They are mostly fits to experimental data without any deeper physical background.

The velocity profile is usually written as a velocity defect law (see equation (1.2)) in this region. To enable a similarity-type description the scaling of the wall-normal coordinate in the outer region must be done with a length scale that is characteristic for the boundary layer thickness. Here we will choose to use the Clauser–Rotta length scale ($\Delta = \delta_* \overline{u}_\infty / u_\tau$, where δ_* is the displacement thickness).

We can now rewrite equation (1.13) (using the boundary condition (1.14)) as

$$\frac{\overline{u}_\infty - \overline{u}_1}{u_\tau} = F(\eta) = C_1 \exp(-C_2\eta) \tag{1.15}$$

where C_1 and C_2 are constants and $\eta = x_2/\Delta$. The validity of the exponential velocity law in the outer region will be tested here against experimental data, and the constants C_1 and C_2 will be determined from the KTH database for zero-pressure-gradient

turbulent boundary layers (Österlund 1999), which covers a Reynolds number range of about $2500 < Re_\theta < 27000$ (based on momentum-loss thickness, θ).

1.3.1. *Derivation of the Reynolds shear stress in the exponential velocity defect region*

The Reynolds shear-stress profile in the region where the velocity defect exhibits an exponential variation can be derived from the mean streamwise momentum equation neglecting the influence of viscosity, along with the continuity equation

$$\overline{u}_1 \frac{\partial \overline{u}_1}{\partial x_1} + \overline{u}_2 \frac{\partial \overline{u}_1}{\partial x_2} = -\frac{\partial \overline{u_1' u_2'}}{\partial x_2}, \tag{1.16}$$

$$\frac{\partial \overline{u}_1}{\partial x_1} + \frac{\partial \overline{u}_2}{\partial x_2} = 0. \tag{1.17}$$

The velocity defect in the outer region is suitably expressed as a function of η (see equation (1.15)). The wall-normal velocity component is calculated using the continuity equation (1.17), assuming a logarithmic velocity profile in the boundary layer below the exponential velocity defect region. This gives an over-estimation of the wall-normal velocity but it is still accurate to first order in $\gamma = u_\tau / U_\infty$. Assuming that the normalized turbulent shear stress is a function of η,

$$-\frac{\overline{u_1' u_2'}}{u_\tau^2} = g(\eta), \tag{1.18}$$

we obtain the following momentum equation to zeroth order in γ:

$$g'(\eta) = H_{12} \eta F'(\eta), \tag{1.19}$$

where a prime denotes differentiation with respect to η and $H_{12} = \delta_*/\theta$ is the shape factor. Note that the right-hand side of equation (1.19) originates from the advection term, i.e. from non-parallel flow effects. Under the parallel flow assumption the solution for $g(\eta)$ is simply a constant, i.e. the well-known solution for the overlap region. The first-order correction to this solution outside the overlap region may be found by use of the previously derived exponential solution for $F(\eta)$ in (the inner part of) the wake region.

We also note from the form of equation (1.19) that the normalization of the velocity defect with u_τ together with the scaling of the wall-normal distance with the Clauser–Rotta length scale, Δ, gives a consistent similarity form of the momentum equation. We may expand $g(\eta)$ in the parameter γ, so that

$$g(\eta) = g_0(\eta) + \gamma g_1(\eta) + O(\gamma^2). \tag{1.20}$$

The zeroth-order solution is found by inserting $g(\eta) = g_0(\eta)$ and the exponential velocity defect law into equation (1.19). The resulting equation has the following solution:

$$g_0(\eta) - g_0(\eta_0) = H_{12} \frac{C_1}{C_2} [(C_2 \eta + 1) \exp(-C_2 \eta) - (C_2 \eta_0 + 1) \exp(-C_2 \eta_0)]. \tag{1.21}$$

The derivation of the equation for $g(\eta)$, and its solution are described in some detail in Appendix B.

1.3.2. *Two-point correlation functions in the exponential velocity defect region*

A further step in the investigation of the new scaling laws derived from Lie group symmetry methods is to look at the two-point correlation functions in the wake

region. The equation for the two-point correlation function, neglecting viscosity, in a zero-pressure-gradient turbulent boundary layer can be expressed as

$$\frac{\mathrm{D}R_{ij}}{\mathrm{D}t} = -R_{kj}\frac{\partial \overline{u}_i}{\partial x_k} - R_{ik}\left.\frac{\partial \overline{u}_j}{\partial x_k}\right|_{x+r} - (\overline{u}_k(\boldsymbol{x}+\boldsymbol{r}) - \overline{u}_k(\boldsymbol{x}))\frac{\partial R_{ij}}{\partial r_k}$$
$$+ \text{(terms containing pressure–velocity correlations and triple correlations)}. \quad (1.22)$$

Under the assumption of parallel shear flow, i.e. $\overline{u}_i = \delta_{i1}\overline{u}_1(x_2)$, the above equation reduces to

$$0 = -\delta_{i1}R_{2j}\frac{\partial \overline{u}_1}{\partial x_2} - \delta_{j1}R_{i2}\left.\frac{\partial \overline{u}_1}{\partial x_2}\right|_{x_2+r_2} - (\overline{u}_1(x_2+r_2) - \overline{u}_1(x_2))\frac{\partial R_{ij}}{\partial r_1}$$
$$+ \text{(terms containing pressure–velocity correlations and triple correlations)}. \quad (1.23)$$

Note here that if the wall-normal separation, r_2, is zero the streamwise–streamwise correlation component, R_{11}, does not appear in the equation, i.e. this equation then yields no information regarding the scaling of the R_{11}-component.

Returning to the characteristic equation (1.6) we can see that the two-point correlation function, assuming inhibited scaling of x_2 in the outer region, giving $k_{s_1} = 0$, yields the following expressions for r_i and R_{ij}:

$$\tilde{r}_i = r_i, \quad (1.24)$$

$$\frac{\mathrm{d}R_{ij}}{\mathrm{d}x_2} = -2\frac{k_{s_2}}{k_{x_2}}R_{ij}. \quad (1.25)$$

Solving the equation for R_{ij} gives an exponential behaviour of the correlation functions with twice the exponent compared to that for the velocity defect (equation (1.15)) i.e.

$$R_{ij} = \tilde{R}_{ij}(\boldsymbol{r})\exp(-2C_2\eta). \quad (1.26)$$

Modifications of this form due to non-parallel flow and other effects are discussed in conjunction with the presentation of experimental data in § 2.5.

2. Results

Here we will test the scaling laws derived in the previous section against experimental data from the KTH database. Also, some DNS data will be analysed for the same purpose. The focus is on the zero-pressure-gradient turbulent boundary layer. Scaling laws for other flows and flow quantities can also be derived with the Lie group symmetry method (see Oberlack 2001 and Cantwell 2002).

2.1. *A modified log-law just below the overlap region*

The form of the velocity distribution in the region inside the overlap region (sufficiently far from from the wall for the viscous stress to be negligible) is predicted to take the form of equation (1.9). With a positive value of A^+, such a form should give a small overshoot (relative to the standard log-law) just below the universal overlap region. Such a behaviour has been observed in many experimentally obtained mean velocity profiles for turbulent boundary layers. A sample profile from the KTH database is shown in figure 1.

A small overshoot around (or just below) $x_2^+ = 100$ is clearly seen. Similar results can be found in other experiments and simulations. See e.g. figure 1 in Zagarola, Perry & Smits (1997) and figure 1 in Perry, Hafez & Chong (2001) with data from pipe flow. See also figure 3.3 in Österlund (1999) and the earlier work by e.g. Smith &

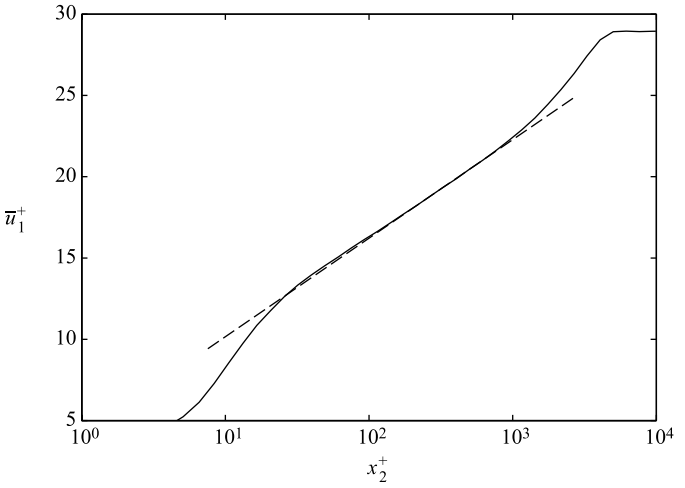

FIGURE 1. Streamwise mean velocity profile in inner scaling from Österlund (1999). Note the 'hump' in the inner part of the log region. (Dashed line: log-law with $\varkappa = 0.38$, $B = 4.1$.) $Re_\theta = 14300$.

Walker (1959). The data here is from boundary layer flow, but it can also be seen in some direct numerical simulations of turbulent channel flow, e.g. Moser, Kim & Mansour (1999). There are (at least) three possible explanations for this observation of overshoot in experimental data.

An inaccuracy in the probe position relative to the wall can give an offset in x_2 that enters the log-law exactly in the same way as the constant A in this case. However, it seems unlikely that all investigators would over-estimate the distance between the probe and the wall. Another explanation is that if the mean profile is determined using a pitot tube, the streamwise velocity is over-predicted in this region. Compensation for this phenomenon is included in many pitot tube calibration functions. A third possibility is that it is coupled to the A-constant in the law (1.9). The accuracy of the hot-wire data of Österlund (1999) has been analysed in detail and the magnitude of the overshoot is larger than any possible inaccuracy of the measurements. For instance, the distance to the wall was determined there to within a few 'plus' units.

A sensitive measure to test the possibility of a modified log-law is the diagnostic function Ξ

$$\Xi = \left(x_2^+ \frac{\mathrm{d}\overline{u}_1^+}{\mathrm{d}x_2^+} \right)^{-1}. \tag{2.1}$$

This quantity was evaluated from the ensemble of velocity profiles of the KTH database, which covers momentum-loss Reynolds numbers from about 2500 to 27000. The details of the evaluation of this quantity are described in Österlund *et al.* (2000*b*). It is plotted in figure 2. It should be constant and equal to the Kármán constant if the log-law is valid. As we can see, the classical log-law is valid down to about $x_2^+ = 200$. With the addition of the constant A^+ the modified log-law should give a diagnostic function that follows the function $\varkappa(1 + A^+/x_2^+)$. As is seen in figure 2, this may be said to be valid down to about $x_2^+ = 100$ if A^+ is set to 5. Österlund *et al.* (2000*b*) define the inner limit of the universal overlap region to be about $x_2^+ = 200$. We see that the influence of the additive constant is essentially below that limit. The choice

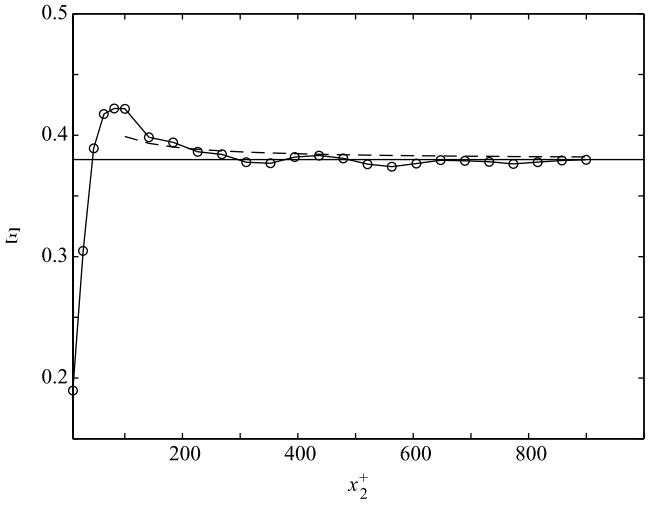

FIGURE 2. The diagnostic function, Ξ; data averaged from experiments by Österlund (1999) (circles), $\Xi = \varkappa$ (solid line) and the modified law $\Xi = \varkappa(1 + A^+/x_2^+)$ (dashed line), with $\varkappa = 0.38$ and $A^+ = 5$.

of 5 for the value of A^+ can be regarded as somewhat arbitrary since the fit to the experimentally found 'hump' in figure 2 is of a more qualitative character.

We should note that the modified log-law cannot be part of the actual overlap region since it has a form that cannot be matched with the formulation in outer scaling. This is consistent with the finding that it only influences the mean profile below the inside limit of the universal overlap region as defined by Österlund *et al.* (2000*b*).

In direct numerical simulations of channel flow by Moser *et al.* (1999) the diagnostic function Ξ has a similar behaviour to the experimental data in figure 2 but without a proper log region due to the low Reynolds number. This is seen as a dip in the plot of $1/\Xi$ in figure 2 of that paper. Similar trends in the behaviour of Ξ are also found in data from the super-pipe experiment by Zagarola, Perry & Smits (1997) (and corrected data presented at the IUTAM Symposium, Princeton, USA, Sept. 2002).

2.2. *The two-point correlation function, R_{12}, in the overlap region*

The streamwise–wall-normal component of the two-point correlation function normalized with the friction velocity squared, i.e.

$$R_{12}^*(\boldsymbol{x}, \boldsymbol{r}) = \frac{\overline{u_1'(\boldsymbol{x}, t) u_2'(\boldsymbol{x} + \boldsymbol{r}, t)}}{u_\tau^2}, \tag{2.2}$$

where $*$ denotes normalization with u_τ^2, was calculated for a number of separations in the streamwise direction using Taylor's hypothesis. Taylor's hypothesis of frozen turbulence ($\Delta x_1 = \overline{u}_1 \Delta t$) is used throughout this paper whenever correlation functions are calculated. The use of Taylor's hypothesis to achieve a chosen separation between the points in the correlation function will of course be a limiting factor in some parts of the flow where the fluctuation intensity is large compared to the mean velocity. In the log-layer $u_{2\mathrm{rms}}/\overline{u}_1$ is fairly small (about 5–8%) and Taylor's hypothesis should be expected to work well.

From the characteristic equation (1.6), we saw in the previous section that the two-point correlation should depend on the variable, r_k/x_2, alone see equation (1.11).

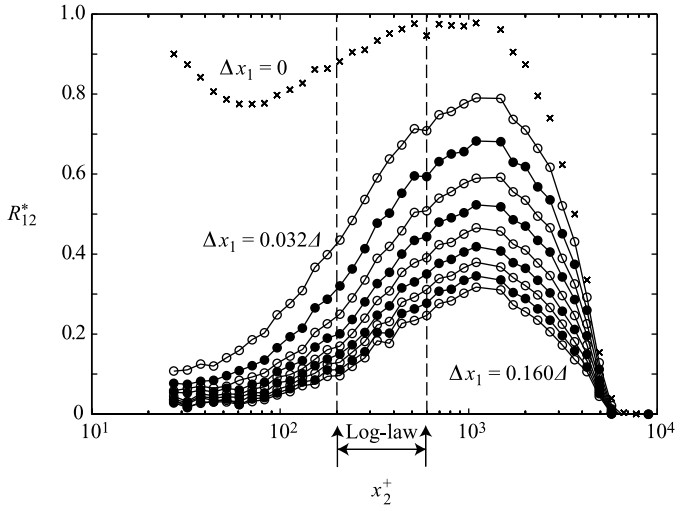

FIGURE 3. The R_{12}^* correlation function plotted against wall distance in inner scaling for varying separation. Non-zero separations ($\Delta x_1/\Delta = 0.032$, 0.048, 0.064, 0.080, 0.096, 0.112, 0.128, 0.144, 0.160) are estimated by use of Taylor's hypothesis. $Re_\theta = 17600$.

Here we use a separation vector $r_k = \Delta x_1 \delta_{k1}$. In figure 3, the R_{12}^* correlation function (normalized by u_τ) is plotted against the normalized wall-normal distance. As we can see, the correlation function for large separations behaves in a functional manner similar to that for zero separation ($\overline{u_1' u_2'}/u_\tau^2$) although the magnitude in the inner near-wall region decreases rapidly as the wall is approached for the case of large separations. This is a natural consequence of the fact that the large-scale structures are predominantly found away from the wall, in the outer region. Furthermore since the separations are large and the information associated with R_{12}^* therefore is of large scale the accuracy of the experimentally determined curves should be very good since the problems with spatial resolution are negligible in this case.

When plotting R_{12}^* against $\Delta x_1/x_2$, as suggested by Lie group symmetry scaling (equation (1.11)), the data collapse for the points from the logarithmic overlap region. This is shown in figure 4 where the filled circles represent experimental data points within the overlap region. The good agreement between the theory, developed using the parallel flow assumption, and the experimental data strongly supports that this assumption is valid in the logarithmic overlap region.

2.3. *An exponential mean velocity defect variation in the wake region*

The mean streamwise velocity profiles from the KTH database (Österlund 1999) used here cover a wide range of Reynolds numbers. In figure 5, 70 of these profiles, with Reynolds number based on the momentum-loss thickness ranging from 2500 to 27000, are plotted in outer scaling, i.e. as the velocity defect against the wall-distance normalized by the Clauser–Rotta boundary layer thickness. Despite the large number of profiles, we can observe a very good collapse of the data. In the log-lin plot there is a substantial range where the data fall onto a straight line, i.e. where the velocity defect exhibits an exponential variation with wall distance. The exponential velocity law (1.15) closely fits the data in the range of about $0.025 \leqslant x_2/\Delta \leqslant 0.11$ with the constants determined as

$$C_1 = 10.5, \quad C_2 = 9.5. \tag{2.3}$$

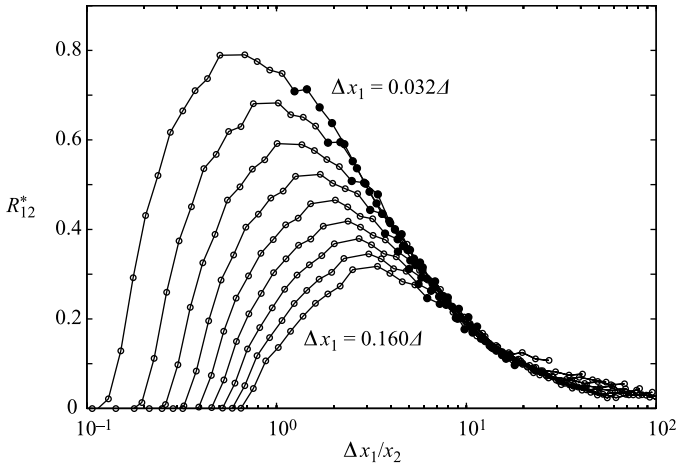

FIGURE 4. The R_{12}^* correlation plotted against separation scaled with wall distance. Filled symbols (circles) represent points within the log-layer ($x_2^+ > 200$ and $x_2/\delta_{95} < 0.15$). Separations ($\Delta x_1/\Delta = 0.032$, 0.048, 0.064, 0.080, 0.096, 0.112, 0.128, 0.144, 0.160) are estimated by use of Taylor's hypothesis. $Re_\theta = 17600$.

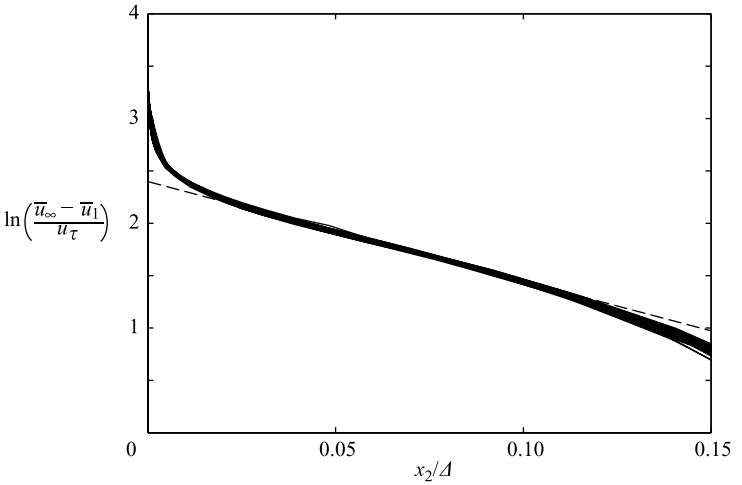

FIGURE 5. 70 mean velocity profiles from Österlund (1999) with $2530 < Re_\theta < 27300$ and the exponential wake law (dashed line).

One should keep in mind that to translate the wall distances normalized by the Clauser–Rotta boundary layer thickness to x_2/δ_{99} one should multiply by a factor of roughly 4.5, which means that the close fit covers a range of about $0.11 \leqslant x_2/\delta_{99} \leqslant 0.50$ ($0.14 \leqslant x_2/\delta_{95} \leqslant 0.63$ and $0.09 \leqslant x_2/\delta_C \leqslant 0.42$ where δ_C is the Coles thickness, see Coles 1956). Hence, this range corresponds to almost half the boundary layer thickness. It is thereby substantially larger than the region with a logarithmic velocity law.

The innermost part with an exponential velocity-defect variation corresponds approximately to the end of the overlap region, where the velocity defect has a logarithmic variation. It may seem surprising that these two rather different types of velocity law can meet. There is no strict matching between the two, but to illustrate the situation the logarithmic velocity defect law found by Österlund *et al.* (2000*b*) is

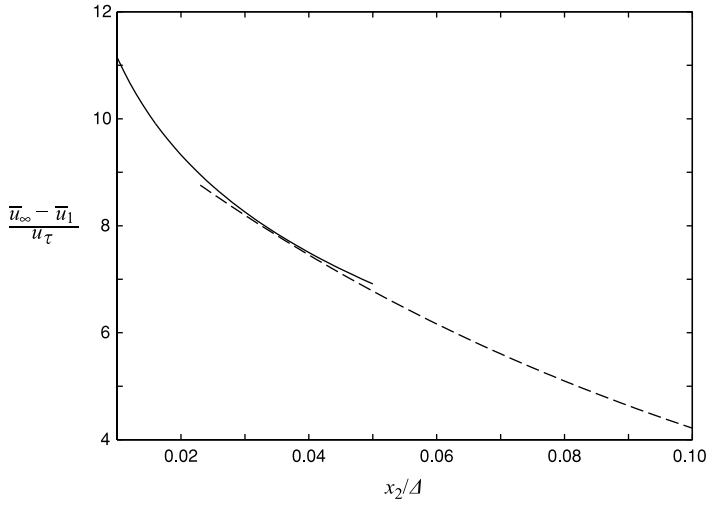

FIGURE 6. The log-law (solid curve), with $\varkappa = 0.38$ and $B = -0.97$ and the exponential wake law (dashed curve), with $C_1 = 10.9$ and $C_2 = 9.5$, versus wall distance in outer scaling.

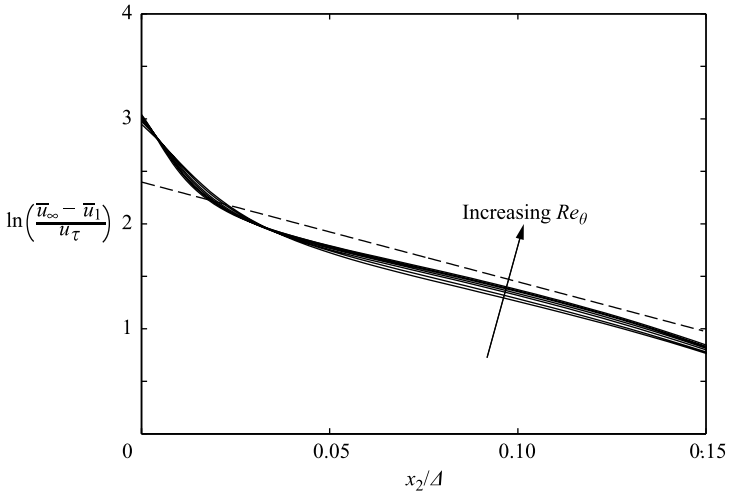

FIGURE 7. Direct numerical simulation data (seven profiles) from Skote (2001) for the velocity defect in boundary layer flow with $380 < Re_\theta < 710$ compared to the exponential wake law (dashed line).

plotted together with the exponential law (1.15) in figure 6. Note that the exponential law is not located in an overlap region in the matching between the inner and outer flow regions. It is completely contained within the outer region. In figure 6 it can be seen that the solid curve representing the log-law and the dashed curve representing the wake law meet at an x_2/Δ of about 0.035. The derivative of the functions is the same here as well. The transition between the two forms is, hence, smooth, although some adjustment region must exist to match higher-order derivatives between the two forms. The location of the transition is also consistent with the outer limit of the log-layer as determined by Österlund *et al.* (2000*b*).

As seen in figure 5, this set of experimental data with moderate to high Reynolds numbers closely follows the exponential velocity defect law. In figure 7 data from

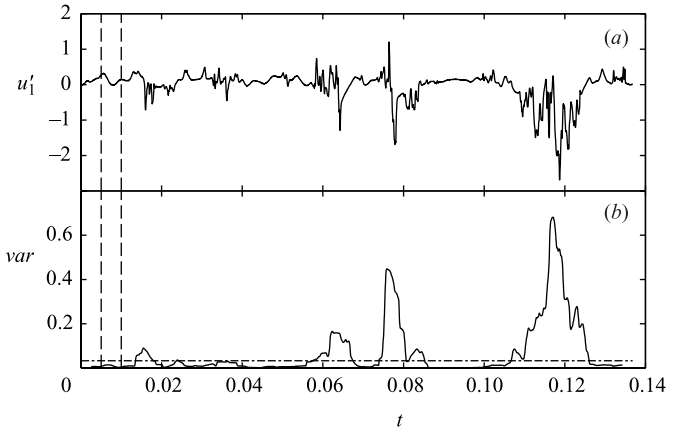

FIGURE 8. (*a*) Time-series of the streamwise velocity signal. (*b*) Short-time variance of the velocity time series in (*a*). The vertical dashed lines show the size of the short-time-variance time window, T. The horizontal dashed line is the short-time-variance threshold, $k = 0.1u_{1\mathrm{rms}}^2$.

Skote (2001) from a direct numerical simulation of a zero-pressure-gradient turbulent boundary layer flow is plotted together with the exponential law. The Reynolds number based on the momentum-loss thickness varies from 380 to 710. The data approach the exponential velocity defect law with increasing Reynolds number, but the curves are not quite straight at these low Reynolds numbers.

In the outermost part of the wake region the velocity defect decreases more rapidly than predicted by the exponential velocity defect law (see figure 5). A possible reason for this behaviour is that the relative influence of viscosity may be higher in this region than otherwise in the outer region. In this paper we will attempt to investigate this possibility further. Another possible explanation is that undisturbed free-stream fluid penetrates the boundary layer to give an intermittent behaviour. Since this fluid has a higher velocity than the local mean of the turbulent flow, the mean velocity increases and thereby the velocity defect decreases. The region of the boundary layer affected by the intermittency can be identified by the high flatness factor found there. The influence of intermittency is checked in this paper using experimental boundary layer data from the KTH database.

In figure 8 a time trace of a hot-wire signal at $x_2/\Delta = 0.272$ is shown together with the short-time variance of the same signal. The free-stream parts of the signal can clearly be seen here as flat regions where the mean velocity is also higher than in the turbulent parts. The flatness at this wall-normal position is about ten times higher than in the log-layer, which indicates a very high degree of intermittency.

The influence of the intermittency on the velocity defect was investigated through the removal of the free-stream parts of the velocity time signal using a short-time variance scheme. The idea is to locate the parts of the time signal with free-stream behaviour, using a running variance window, since the free-stream parts of the time signal have very low variance compared to the turbulent parts. A threshold, k, determines whether the given sample is kept or discarded. The short-time variance (see Blackwelder & Kaplan 1976) is defined as

$$var = \frac{1}{T}\int_{t-T/2}^{t+T/2} u_1^2(s)\,\mathrm{d}s - \left(\frac{1}{T}\int_{t-T/2}^{t+T/2} u_1(s)\,\mathrm{d}s\right)^2, \tag{2.4}$$

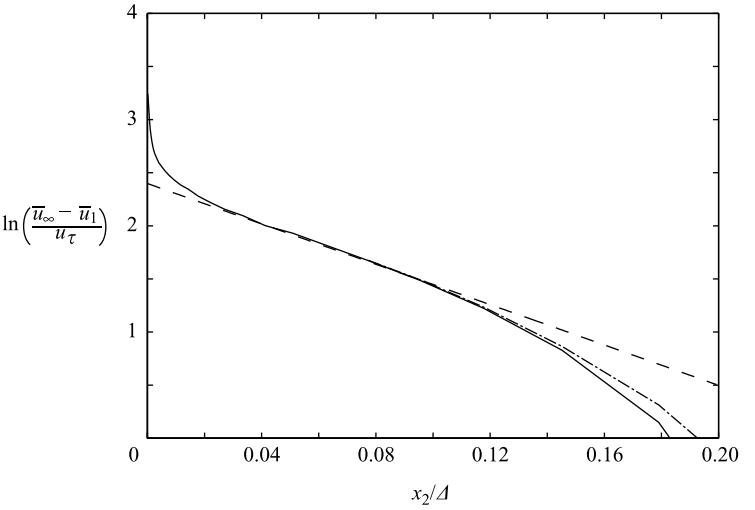

FIGURE 9. A mean velocity defect profile from Österlund (1999) at $Re_\theta = 9600$ (solid line), and compensated for intermittency (dash-dotted line), and the exponential velocity defect law (dashed line).

where T is the time window over which the variance is calculated. The parts where the variance is lower than $0.1u_{1\mathrm{rms}}^2$ were removed when the new mean value of the streamwise velocity was calculated. In figure 8 the threshold level is shown as a horizontal dash-dotted line. The two vertical dashed lines indicate the size of the time window, T, used to calculate the short-time variance.

As expected from the short sample in figure 8 the removal of the free-stream parts from the velocity time series decreases the streamwise velocity and thus increases the velocity defect at the wall-normal positions with high flatness, see figure 9. Otherwise the changes are small. The intermittency phenomenon does not, however, seem to be the major factor in explaining the rapid decrease of the velocity defect.

It has been suggested that the relative influence of viscosity in the outer part of the boundary layer is high and that this could contribute to the fast approach of the velocity profile towards the free-stream value. A first check is to evaluate whether the viscous stresses can be neglected compared to the Reynolds stresses in the outermost region. If this were not the case the inviscid approximation used to derive the scaling laws would be inappropriate, and this could be a contributing factor to the experimental data deviation from the exponential velocity defect law. In figure 10 we have calculated the ratio of the Reynolds shear stress, $-\rho\overline{u_1 u_2}$, and the viscous stress, $\mu \mathrm{d}\overline{u}_1/\mathrm{d}x_2$ for a number of different Reynolds numbers ($6900 < Re_\theta < 22600$). The result indicates that the viscous stress is much smaller than the Reynolds shear stress in the wake outside the region with an exponential velocity defect. The conclusion is therefore that the reason for the exponential defect law failing outside $x_2/\Delta = 0.12$ has to be found elsewhere, and most probably in effects of non-parallel flow. In § 2.5, this will be discussed further in connection with the evaluation of two-point correlation data.

2.4. *Reynolds shear stress in the exponential velocity defect region*

The Reynolds-shear-stress profile corresponding to the exponential form of the velocity defect law was derived in § 1.3.1 (and Appendix B). The solution to zeroth order in γ for the normalized shear stress $(-\overline{u_1' u_2'}/u_\tau^2)$ is shown for two different

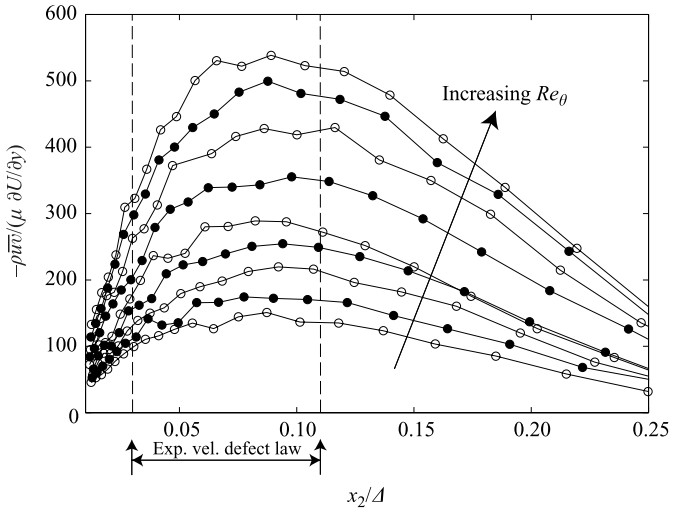

FIGURE 10. The ratio between the Reynolds stress and the viscous stress at $6900 < Re_\theta < 22600$. The open and filled symbols are used to facilitate the interpretation of the figure.

Reynolds numbers ($Re_\theta = 6930$ and $Re_\theta = 22530$) in figure 11. We see that this solution has the correct functional behaviour in the region with exponential velocity defect but that the error in magnitude is of order γ.

The solution for $g(\eta)$ that is accurate to first order in γ (see Appendix B) is of similar form to $g_0(\eta)$. As seen in figure 11, it represents the Reynolds shear stress accurately in the region where an exponential behaviour of the velocity defect can be observed.

2.5. *Testing of theoretical predictions for two-point correlation functions in the exponential velocity defect region*

As described in § 1.3.2 the form of the two-point correlation tensor, R_{ij}, that corresponds to the exponential velocity defect law is given by equation (1.15). The assumption of parallel shear flow implies that the evolution equation for R_{ij} does not give any information regarding the scaling of R_{11}. It may still be interesting to study its behaviour, however. Normalized by u_τ^2 it is plotted in figure 12 as function of wall distance, η, for various (large) separations. Here as well as in the following figures the streamwise separation is calculated by use of Taylor's hypothesis. The separations analysed are chosen to be similar in size to typical wall-normal distances in the region investigated, namely the exponential defect region. Hence, these separations should be large enough to be associated with inviscid dynamics. We can observe a variation that is close to an exponential one. A closer look at the slope of the straight lines in figure 12 shows (see figure 13) that the slope is far from constant and far from the value $2C_2 \approx 19$ in equation (1.15).

For the other two measured components of the two-point correlation function the exponential behaviour as written in equation (1.26) is expected to describe the spatial variation of the experimental data. Figures 14 and 15 show that this expectation does not hold. The predicted behaviour is a rapid exponential decrease (with a $-2C_2$ slope) with increasing distance from the wall. This is certainly not observed. In fact, neither of them show any tendency towards an exponential form in the velocity defect region. The most plausible candidate for the cause of deviation from exponential behaviour

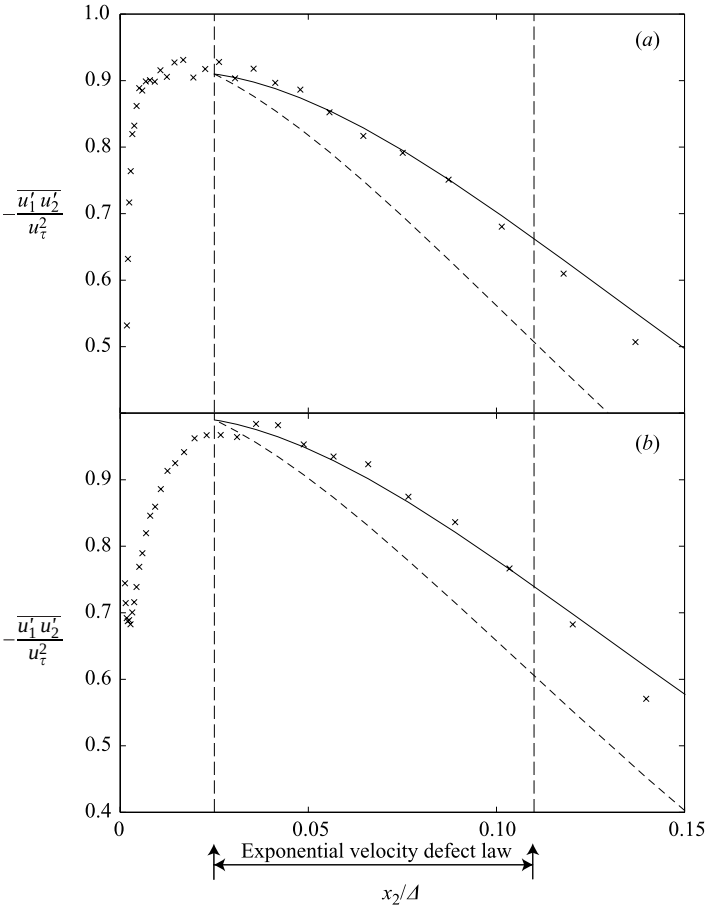

FIGURE 11. (*a*) Normalized Reynolds shear stress at $Re_\theta = 6930$. (*b*) Normalized Reynolds shear stress at $Re_\theta = 22530$. Solid and dashed curves represent the derived expressions for the normalized Reynolds shear stress that are accurate to first and zeroth order in γ, respectively. The integration constants $g_0(\eta_0) = 0.91$ (*a*) and $g_0(\eta_0) = 0.99$ (*b*) and $g_1(\eta_0) = 0$ (*a*, *b*) have been chosen to give the best fit to the experimental data. $\eta_0 = 0.025$.

in the velocity defect and the correlation function is related to effects of non-parallel flow in the wake region of the boundary layer flow. The effect on the correlation function is seen to be much stronger than for the velocity defect.

The effect of non-parallel flow in a boundary layer increases with wall distance. In the overlap region the degree of non-parallel flow is very small, which is supported by the fact that the theoretically predicted dependence of the R_{12} correlation was shown to agree well with experimental data. However, in the outermost part of the boundary layer the relative importance of non-parallel effects grows. Therefore, the left-hand side of the equation for the correlations, (1.22), can no longer be neglected as is the case when the parallel flow assumption is valid.

Now, assume that the correlation function is a function of η and $\boldsymbol{r}$, i.e.

$$R_{ij} = R_{ij}(\eta, \boldsymbol{r}). \tag{2.5}$$

The validity of the assumption of this form can be debated, and we will return to its consequences later. We here use this form to simplify the analysis and it is probably

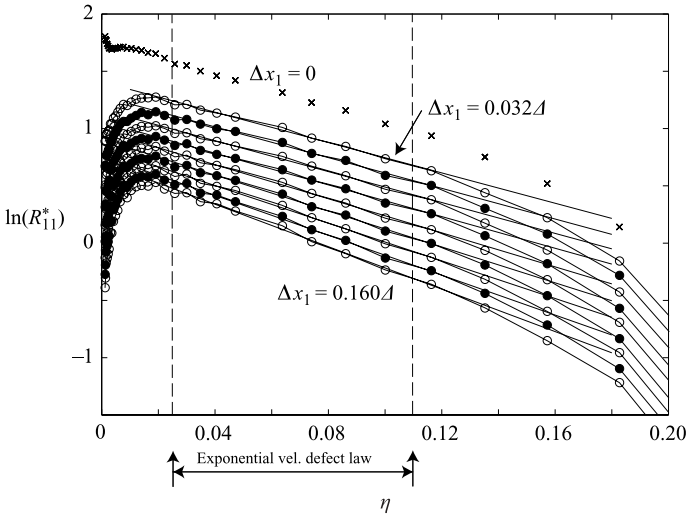

FIGURE 12. R_{11}^* in the wake region. Solid lines are least-square fits to the data within the exponential wake region ($0.03 < x_2/\Delta < 0.12$); $\times$, zero separation ($\overline{u_1 u_1}/u_\tau^2$). Non-zero separations, ($\Delta x_1/\Delta = 0.032, 0.048, 0.064, 0.080, 0.096, 0.112, 0.128, 0.144, 0.160$) are estimated by use of Taylor's hypothesis. $Re_\theta = 17300$.

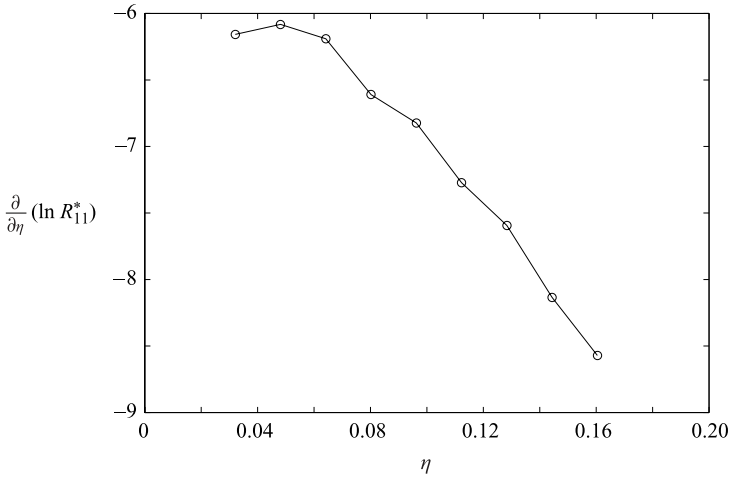

FIGURE 13. The variation of the slope of the least-square-fitted solid lines in figure 12 with wall distance.

sufficient to yield useful information about the importance of non-parallel effects in the outer part of the wake region. We can now rewrite equation (1.22) with the above assumption, also assuming steady state and a velocity defect form of the mean velocity description. The resulting equation (to zeroth order in γ) is

$$\eta\frac{\partial R_{ij}}{\partial\eta} = -\delta_{i1}R_{2j}F'(\eta) - \delta_{j1}R_{i2}F'\left(\eta+\frac{r_2}{\Delta}\right) - \left(F\left(\eta+\frac{r_2}{\Delta}\right) - F(\eta)\right)\frac{1}{\Delta}\frac{\partial R_{ij}}{\partial r_1}$$
$$+ \text{(terms containing pressure–velocity correlations and triple correlations).} \quad (2.6)$$

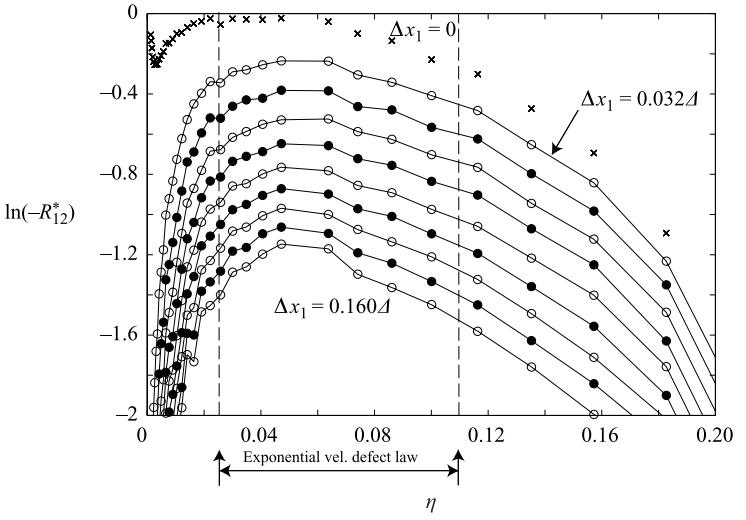

FIGURE 14. R_{12}^* in the wake region; ×, zero separation ($\overline{u_1 u_2}/u_\tau^2$). Non-zero separations, ($\Delta x_1/\Delta = 0.032$, 0.048, 0.064, 0.080, 0.096, 0.112, 0.128, 0.144, 0.160) are estimated by use of Taylor's hypothesis. $Re_\theta = 17300$.

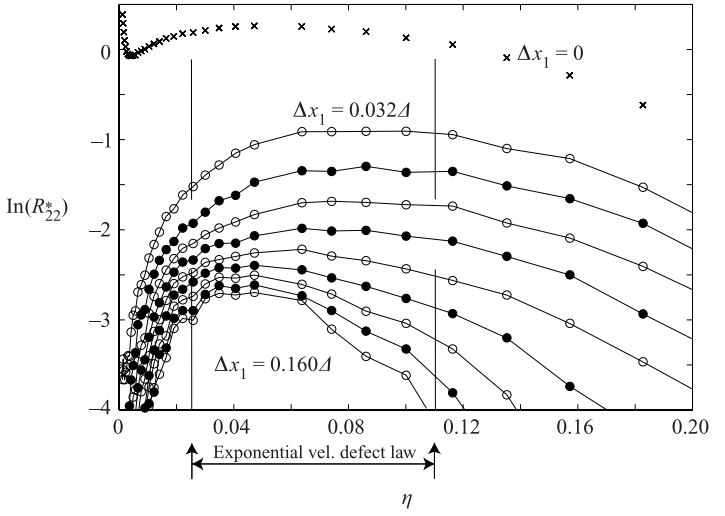

FIGURE 15. R_{22}^* in the wake region; ×, zero separation ($\overline{u_2 u_2}/u_\tau^2$). Non-zero separations, ($\Delta x_1/\Delta = 0.032$, 0.048, 0.064, 0.080, 0.096, 0.112, 0.128, 0.144, 0.160) are estimated by use of Taylor's hypothesis. $Re_\theta = 17300$.

Considering the case when the wall-normal separation is zero, i.e. $r_2 = 0$, we obtain the following equations for the correlation functions:

$$\eta \frac{\partial R_{11}}{\partial \eta} = -2R_{12}F'(\eta) + (\text{terms containing pressure–velocity and triple corr.}), \quad (2.7)$$

$$\eta \frac{\partial R_{12}}{\partial \eta} = -R_{22}F'(\eta) + (\text{terms containing pressure–velocity and triple corr.}), \quad (2.8)$$

$$\eta \frac{\partial R_{22}}{\partial \eta} = 0 + (\text{terms containing pressure–velocity and triple correlations}). \quad (2.9)$$

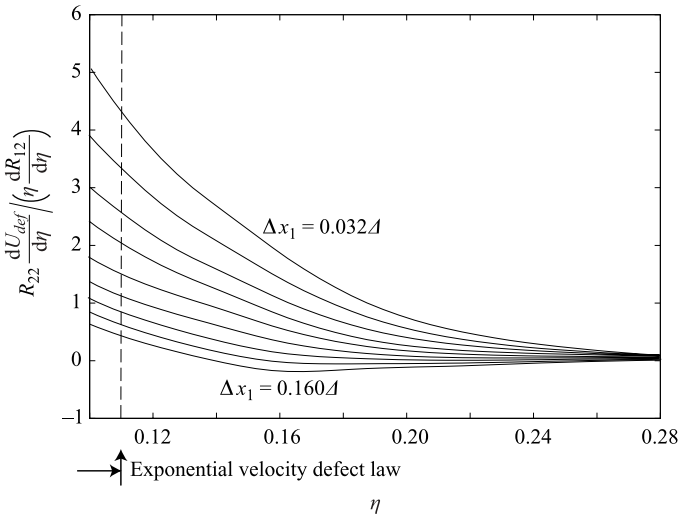

FIGURE 16. Ratio between production and advection terms in the transport equation for R_{12}. The velocity defect and the correlation functions have been smoothed and interpolated here to facilitate differentiation. $Re_\theta = 17300$.

Note here that $R_{12} = R_{21}$ in equation (2.7) because the separation in the wall-normal direction is zero.

To test the influence of non-parallel flow the ratio of the production term on the right-hand side in equation (2.8) and the advection term is calculated from experimental data for various separations. The result is shown in figure 16. For the non-parallel effects to be important this ratio should be of order unity (or smaller). We see in the figure that the advection term rapidly becomes increasingly important as the boundary layer edge is approached. The influence of the advection term also increases with increasing separation. Note that the curves in figure 16 are curve fits to the experimental correlation function data. This was done to obtain a smoother and clearer picture of the relationship between the terms. It was, however, thoroughly investigated that the gradients calculated using the curve-fitted data were similar to gradients calculated from the original data.

Under different assumptions of the form of R_{ij}, e.g. as $R_{ij}(\eta, \mathrm{r}/\Delta)$, the resulting equations would be somewhat different from equations (2.7)–(2.9). This may indeed be a more natural choice. There would then be contributions to equation (2.8) from other terms related to the new scaling of $\boldsymbol{r}$ that would be more important than the advection term based entirely on η derivatives. These terms would be large enough to balance the production term on the right-hand side in at least parts of the exponential velocity defect region. For both types of R_{ij} forms it seems clear that non-parallel flow effects give a drastically different behaviour of R_{ij} than predicted under the parallel flow assumption.

3. Concluding remarks

The new scaling laws for turbulent boundary layers derived by Oberlack (2001) using Lie group symmetry methods have been tested against the experimental data of the KTH database for turbulent boundary layers with a wide range of Reynolds numbers. A modification of the log-law in the innermost part of the overlap region

could be identified with a constant added to the wall distance in the logarithmic function. With this constant, $A^+ \approx 5$, added, the modified log-law described the experimental data down to $x_2^+ \approx 100$ instead of $x_2^+ \approx 200$ with the standard log-law (where $x_2^+ \approx 200$ was found by Österlund *et al.* 2000*b* as the lower limit of the universal overlap region). The influence of the new constant decreases rapidly away from the wall and is negligible in the universal overlap region. This is consistent with the possibility of matching with the velocity law in outer scaling.

The two-point correlation function in the logarithmic overlap region is predicted by the Lie group symmetry method to be a function of $\Delta x_1/x_2$. This scaling of the wall-normal distance was tested for the R_{12} component using experimental data and it was found that the data collapsed well for points in the overlap region. The good collapse of the data also strongly supports the validity of the assumption of parallel flow in the overlap region.

The new exponential velocity defect law fits the data remarkably well over a large part (roughly half) of the boundary layer thickness. This supports the earlier testing of this law in the work of Oberlack (2001).

An expression for the Reynolds shear stress in the wake region was derived using the exponential velocity defect law. It was found that in the region where this law is valid there was good agreement between the experimental data and the theory if terms of order $u_\tau/\overline{u}_\infty$ are included.

In the outermost part of the boundary layer the predicted exponential velocity defect law deviates substantially from the experimental data. The non-parallel flow effects are the most probable cause of this deviation. These effects were also found to have a major influence on the two-point correlation functions, and their form was found to be quite different from that predicted under the assumption of parallel mean flow.

The authors would like to thank Professor Martin Oberlack for sharing his knowledge on Lie group symmetry methods and discussing the various results in this investigation. Financial support from the Swedish Research Council for the first author is greatfully acknowledged.

Appendix A. Lie group symmetry methods for differential equations

Basic descriptions of symmetry methods for differential equations are given by e.g. Hydon (2000), Oberlack (2001, 2002) and Cantwell (2002). These methods can be viewed as a very general tool for obtaining similarity solutions, or invariants, of differential equations. We will give a brief description below of some of the key elements of such symmetry methods based on continuous Lie groups. An example is similarity-type solutions to partial differential equations, that effectively reduce the number of independent variables. The description below follows that of Oberlack (2002). It is given here to illustrate the foundation of the ideas, in the form of scaling laws, explored in the present paper.

The basic idea of symmetry methods for differential equations is to construct methods of finding transformations of the (ordinary or partial) differential equation that do not change its functional form with the change of variables

$$\boldsymbol{F}(\boldsymbol{x}, \boldsymbol{y}, \boldsymbol{y}_i) = 0 \Leftrightarrow \boldsymbol{F}\left(\boldsymbol{x}^*, \boldsymbol{y}^*, \boldsymbol{y}_i^*\right) = 0 \tag{A 1}$$

where $\boldsymbol{x}$ is the vector of independent variables, $\boldsymbol{y}$ is the vector of dependent variables, index i denotes all derivatives of order i on $\boldsymbol{y}$ and $*$ denotes the transformed variables.

Concentrating our efforts on Lie group symmetries we have analytic transformations that depend on a continuous parameter, ϵ. We write

$$S_\epsilon : \boldsymbol{x}^* = \boldsymbol{\phi}(\boldsymbol{x}, \boldsymbol{y}; \epsilon) \quad \text{and} \quad \boldsymbol{y}^* = \boldsymbol{\psi}(\boldsymbol{x}, \boldsymbol{y}; \epsilon). \tag{A 2}$$

From a Taylor expansion with respect to ϵ we can derive the transformation groups in infinitesimal form,

$$S_\epsilon : \boldsymbol{x}^* = \boldsymbol{x} + \epsilon \boldsymbol{\xi}(\boldsymbol{x}, \boldsymbol{y}) + O(\epsilon^2) \quad \text{and} \quad \boldsymbol{y}^* = \boldsymbol{y} + \epsilon \boldsymbol{\eta}(\boldsymbol{x}, \boldsymbol{y}) + O(\epsilon^2) \tag{A 3}$$

where $\boldsymbol{\xi} = \partial \boldsymbol{\phi} / \partial \epsilon \big|_{\epsilon=0}$ and $\boldsymbol{\eta} = \partial \boldsymbol{\psi} / \partial \epsilon \big|_{\epsilon=0}$ are the so-called infinitesimals.

The striking feature about the Lie group method is that the transformation in infinitesimal form (only terms of order ϵ are kept) is fully equivalent to the transformation in global form (as given by (A 2)). The continuous form can hence be determined from the infinitesimals by integrating the first-order system

$$\frac{\mathrm{d}\boldsymbol{x}^*}{\mathrm{d}\epsilon} = \boldsymbol{\xi}(\boldsymbol{x}^*, \boldsymbol{y}^*), \quad \frac{\mathrm{d}\boldsymbol{y}^*}{\mathrm{d}\epsilon} = \boldsymbol{\eta}(\boldsymbol{x}^*, \boldsymbol{y}^*) \tag{A 4}$$

with initial conditions $\boldsymbol{x}^* = \boldsymbol{x}, \quad \boldsymbol{y}^* = \boldsymbol{y}$ at $\epsilon = 0$.

Furthermore, an important property of Lie groups is that all linear combinations of distinct symmetry groups $S_\epsilon^{(i)}$ also are symmetry groups. This property is also inherited by the infinitesimal form. The superposition property plays a central role in the determination of the scaling laws given in the results section.

To find all symmetries of a differential equation in a rigorous manner, the symmetry condition in equation (A 1) should be written in infinitesimal form (through Taylor expansion). If we restrict ourselves (for algebraic simplicity) to a system of first-order differential equations we may write this as

$$\boldsymbol{F}(\boldsymbol{x}, \boldsymbol{y}, \boldsymbol{y}_1) + \epsilon X \boldsymbol{F}(\boldsymbol{x}, \boldsymbol{y}, \boldsymbol{y}_1) + O(\epsilon^2) = 0. \tag{A 5}$$

We may note that the first term in equation (A 5) is equal to zero, according to equation (A 1), and we can write the symmetry condition in infinitesimal form as follows:

$$X \boldsymbol{F}|_{\boldsymbol{F}=0} = 0. \tag{A 6}$$

X in equations (A 5) and (A 6) is (for a system of first-order differential equations) defined as

$$X = \xi_i \frac{\partial}{\partial x_i} + \eta_j \frac{\partial}{\partial y_i} + \cdots. \tag{A 7}$$

The first terms in equation (A 7) are together called the generator. In a somewhat simplified way we might say that to find the symmetry groups for a particular differential equation one introduces unknown infinitesimals ξ and η into equation (A 6). The result is an over-determined set of linear homogeneous differential equations that is solved for ξ and η. The infinitesimals are then transformed to global form through the Lie differential equation (A 4) with the initial condition given in connection with that equation.

We can define an invariant solution for a partial differential equation like the second equation in (A 1). If this equation admits a symmetry in the form of a generator, X, $\boldsymbol{y} = \Theta(\boldsymbol{x})$ is an *invariant* solution to the partial differential equation if $\boldsymbol{y} - \Theta(\boldsymbol{x})$ is invariant under X, and $\boldsymbol{y} = \Theta(\boldsymbol{x})$ is a solution to the partial differential equation. Using the definition of a generator X from equation (A 7) a hyperbolic system is

obtained,

$$\xi_k(\boldsymbol{x}, \Theta)\frac{\partial \Theta_l}{\partial x_k} = \eta_l(\boldsymbol{x}, \Theta), \tag{A 8}$$

and the corresponding characteristic equation is

$$\frac{\mathrm{d}x_1}{\xi_1(\boldsymbol{x}, \boldsymbol{y})} = \ldots = \frac{\mathrm{d}x_m}{\xi_m(\boldsymbol{x}, \boldsymbol{y})} = \frac{\mathrm{d}y_1}{\eta_1(\boldsymbol{x}, \boldsymbol{y})} = \ldots = \frac{\mathrm{d}y_m}{\eta_m(\boldsymbol{x}, \boldsymbol{y})}. \tag{A 9}$$

Note that here Θ is replaced by $\boldsymbol{y}$.

Oberlack (2002) identifies the symmetries of the Navier–Stokes and Euler equations, and analyses further the symmetries of the differential equation (derived e.g. by Oberlack & Peters 1993) for the two-point correlation tensor, which is defined as

$$R_{ij}(\boldsymbol{x}, \boldsymbol{r}; t) = \overline{u_i'(\boldsymbol{x}; t)\, u_j'(\boldsymbol{x} + \boldsymbol{r}; t)} \tag{A 10}$$

where $\boldsymbol{r}$ is the separation vector.

The Euler equations admit a ten-parameter symmetry group, whereas the viscosity in the Navier–Stokes equations implies a symmetry breaking that reduces this to a nine-parameter group. The elements can be qualitatively described as:

(i) one group that describes translation in time (for which the Euler and Navier–Stokes equations obviously are invariant);

(ii) three rotation groups that simply signify rotation of the coordinate system around each of the three axes (along with corresponding redefinition of the velocity components);

(iii) three groups signifying extended Galilean invariance (in each of the three coordinate directions);

(iv) pressure invariance (under the addition of an arbitrary pressure term that is solely a function of time, or constant);

(v) two groups for the Euler equations and one for the Navier–Stokes equations, describing scaling invariance.

An important feature of analysing the equation for the two-point correlation tensor is that we can study essentially inviscid dynamics by restricting attention to separations that give length scales that are negligibly influenced by viscosity, and at the same time, restricting attention to positions in space where the influence of viscosity (e.g. through viscous stresses) is negligible. This means that all symmetries from the Euler equations carry over to this equation.

Note that this is not the case for the Reynolds stress transport equation, i.e. the single-point limit of the R_{ij}-equation, even if we restrict attention to positions where viscous stresses are negligible.

Hence, the equation for the two-point correlation tensor, admits a ten-parameter symmetry group for length scales (and positions) where the viscous influence is negligible. (The possibility for further symmetry groups of this equation has been investigated by Oberlack and co-workers.) However, restricting ourselves to plane turbulent shear flow with all mean quantities dependent only on the wall-normal coordinate, x_2, leaves us with only four of the original ten symmetries. These symmetries are: the two scaling symmetries, $\overline{X}_{s_1}$ and $\overline{X}_{s_2}$, reduced here due to the one-dimensional mean flow, $\overline{u}_1 = \overline{u}_1(x_2)$; the traditional Galilean invariance in the streamwise direction, $\overline{X}_{\overline{u}_1}$; and the spatial translation symmetry $\overline{X}_{\overline{u}_2}$ (which is the only part left of the extended Galilean invariance in the wall-normal direction).

The symmetry group for the R_{ij}-equation, with the above described restrictions, can then be written as (where terms related to pressure–velocity and triple correlations

have been left out)

$$\overline{X}_{s_1} = x_2\frac{\partial}{\partial x_2} + \overline{u}_1\frac{\partial}{\partial \overline{u}_1} + 2\overline{p}\frac{\partial}{\partial \overline{p}} + r_i\frac{\partial}{\partial r_i} + 2R_{ij}\frac{\partial}{\partial R_{ij}} + \cdots, \tag{A 11}$$

$$\overline{X}_{s_2} = -\overline{u}_1\frac{\partial}{\partial \overline{u}_1} - 2\overline{p}\frac{\partial}{\partial \overline{p}} - 2R_{ij}\frac{\partial}{\partial R_{ij}} + \cdots, \tag{A 12}$$

$$\overline{X}_{\overline{u}_1} = \frac{\partial}{\partial \overline{u}_1}, \tag{A 13}$$

$$\overline{X}_{\overline{u}_2} = \frac{\partial}{\partial x_2}. \tag{A 14}$$

Recalling the superposition property of Lie group algebra, we can combine the four symmetries into

$$\overline{X} = k_{s_1}\overline{X}_{s_1} + k_{s_2}\overline{X}_{s_2} + k_{\overline{u}_1}\overline{X}_{\overline{u}_1} + k_{x_2}\overline{X}_{\overline{u}_2}, \tag{A 15}$$

where k_{s_1}, k_{s_2}, $k_{\overline{u}_1}$ and k_{x_2} are constants (parameters).

We should keep in mind that the above with k_{s_1}, k_{s_2} being independent is only valid in situations where viscous influence is negligible. For cases with significant influence of viscosity it is straightforward to derive the symmetry-breaking relation that requires that $k_{s_2} = 2k_{s_1}$.

The characteristic form of the hyperbolic equation (A 8) for the inviscid case is

$$\frac{\mathrm{d}x_2}{k_{s_1}x_2 + k_{x_2}} = \frac{\mathrm{d}r_{[k]}}{k_{s_1}r_{[k]}} = \frac{\mathrm{d}\overline{u}_1}{(k_{s_1} - k_{s_2})\overline{u}_1 + k_{\overline{u}_1}} = \frac{\mathrm{d}R_{[ij]}}{2(k_{s_1} - k_{s_2})R_{[ij]}} + \cdots, \tag{A 16}$$

where [ ] means that there is no summation over the indices. By changing the values of the two scaling symmetry constants, k_{s_1} and k_{s_2}, scaling laws for different shear-flow situations can be derived.

Appendix B. Derivation of an expression for the Reynolds shear stress in the wake region

Using the exponential velocity defect law, derived by use of Lie group symmetry methods, an expression for the corresponding Reynolds-shear-stress profile is derived here, which is accurate to first order in $\gamma = u_\tau/\overline{u}_\infty$. Perry, Marušić & Li (1994) also treats the case with non-zero pressure gradient with the aim of analysing the attached-eddy hypothesis. The streamwise momentum equation for a zero-pressure-gradient boundary layer, neglecting the viscous stress, and the continuity equation are

$$\overline{u}_1\frac{\partial \overline{u}_1}{\partial x_1} + \overline{u}_2\frac{\partial \overline{u}_1}{\partial x_2} = -\frac{\partial \overline{u_1'u_2'}}{\partial x_2}, \tag{B 1}$$

$$\frac{\partial \overline{u}_1}{\partial x_1} + \frac{\partial \overline{u}_2}{\partial x_2} = 0. \tag{B 2}$$

The velocity defect is defined as

$$\frac{\overline{u}_\infty - \overline{u}_1}{u_\tau} = F(\eta) \tag{B 3}$$

where $\eta = y/\Delta$ and $\Delta = \delta_*/\gamma$ is the Clauser–Rotta boundary layer thickness. Differentiating $\overline{u}_1$ with respect to x_1 and x_2, making use of equation (B 3), yields

$$\frac{\partial \overline{u}_1}{\partial x_1} = -u_\tau\frac{\partial \eta}{\partial x_1}F'(\eta) - \frac{\mathrm{d}u_\tau}{\mathrm{d}x_1}F(\eta) \tag{B 4}$$

for the x_1-derivative and

$$\frac{\partial \overline{u}_1}{\partial x_2} = -\frac{u_\tau}{\Delta} F'(\eta) \tag{B 5}$$

for the x_2-derivative. A prime here denotes differentiation with respect to η. The expression for the x_1-derivative of u_τ can be found from the logarithmic friction law, which was found by Österlund *et al.* (2000*b*), to agree very well with experimental data. It is

$$\frac{u_\tau}{\overline{u}_\infty} = \left(\frac{1}{\varkappa} \ln Re_\theta + C\right)^{-1}. \tag{B 6}$$

Differentiating equation (B 6) with respect to x_1 and multiplying with θ gives

$$\frac{\theta}{\overline{u}_\infty}\frac{\mathrm{d}u_\tau}{\mathrm{d}x_1} = -\theta\left(\frac{1}{\varkappa} \ln Re_\theta + C\right)^{-2} \frac{1}{\varkappa\theta}\frac{\mathrm{d}\theta}{\mathrm{d}x_1} = -\frac{\gamma^4}{\varkappa} \tag{B 7}$$

since

$$\frac{\mathrm{d}\theta}{\mathrm{d}x_1} = \gamma^2 \tag{B 8}$$

for a zero-pressure-gradient boundary layer.

We will also need $\mathrm{d}\delta_*/\mathrm{d}x_1$ below, which we can write as

$$\frac{\mathrm{d}\delta_*}{\mathrm{d}x_1} = \frac{\mathrm{d}(H_{12}\theta)}{\mathrm{d}x_1} = H_{12}\gamma^2 + \theta\frac{\mathrm{d}H_{12}}{\mathrm{d}x_1}. \tag{B 9}$$

By inserting the definition (B 3) into the expressions for δ_* and θ we readily obtain

$$H_{12} = \int_0^\infty F(\eta)\mathrm{d}\eta \Big/ \left(\int_0^\infty F(\eta)\mathrm{d}\eta - \gamma\int_0^\infty F^2(\eta)\mathrm{d}\eta\right) = 1\Big/\left(1 - \gamma\int_0^\infty F^2(\eta)\mathrm{d}\eta\right) \tag{B 10}$$

where the second identity follows from the definition of Δ. Hence we obtain (by use of equation (B 7)),

$$\frac{\mathrm{d}H_{12}}{\mathrm{d}x_1} = -\frac{H_{12}^2}{\varkappa\theta}\gamma^4\int_0^\infty F^2(\eta)\mathrm{d}\eta \tag{B 11}$$

and thereby

$$\frac{\mathrm{d}\delta_*}{\mathrm{d}x_1} = H_{12}\gamma^2 + O(\gamma^4). \tag{B 12}$$

We can now compute the derivatives of η as

$$\frac{\partial\eta}{\partial x_1} = -\frac{\eta}{\Delta}\frac{\mathrm{d}\Delta}{\mathrm{d}x_1} = -\frac{\eta}{\Delta}\left(\frac{1}{\gamma}\frac{\mathrm{d}\delta_*}{\mathrm{d}x_1} - \frac{\delta_*\overline{u}_\infty}{u_\tau^2}\frac{\mathrm{d}u_\tau}{\mathrm{d}x_1}\right) = -\frac{\eta}{\Delta}H_{12}\gamma\left(1 + \frac{1}{\varkappa}\gamma + O(\gamma^2)\right) \tag{B 13}$$

and

$$\frac{\partial\eta}{\partial x_2} = \frac{1}{\Delta}. \tag{B 14}$$

Multiplying with Δ/u_τ and making use of equations (B 13) and (B 7) we can rewrite expression (B 4) as

$$\frac{\Delta}{u_\tau}\frac{\partial\overline{u}_1}{\partial x_1} = H_{12}\gamma\left(\eta F'(\eta) + \frac{1}{\varkappa}\gamma(\eta F(\eta))' + O(\gamma^2)\right) \tag{B 15}$$

and (B 5) as

$$\frac{\Delta}{u_\tau}\frac{\partial \overline{u}_1}{\partial x_2} = -F'(\eta). \tag{B 16}$$

Finally, to complete the left-hand side of equation (B 1) it also necessary to calculate $\overline{u}_2$. Using the continuity equation (B 2) and equation (B 15) we can express $\overline{u}_2$ as

$$\overline{u}_2 - \overline{u}_{2_0} = -u_\tau H_{12}\gamma \left\{ \int_{\eta_0}^{\eta} \xi F'(\xi)\mathrm{d}\xi + O(\gamma) \right\}, \tag{B 17}$$

where η_0 is chosen here as the outer limit of the log-layer. To estimate $\overline{u}_{2_0}$ we assume a logarithmic velocity defect law, $F_{log}(\eta)$, in the region $0 < \eta < \eta_0$,

$$F_{log}(\eta) = -\frac{1}{\varkappa}\ln\eta + C, \;\; \eta \leqslant \eta_0. \tag{B 18}$$

This assumption will overestimate $\overline{u}_{2_0}$ with an error in $\overline{u}_{2_0}$ of order γ^2. Introducing equation (B 18) into the continuity equation, (B 2), and integrating gives the following expression for $\overline{u}_{2_0}$:

$$\overline{u}_{2_0} = H_{12}\frac{u_\tau\gamma}{\varkappa}\eta_0 + O(\gamma^2). \tag{B 19}$$

Furthermore, it is assumed that the Reynolds shear stress normalized with u_τ^2 is a function of η, i.e.

$$g(\eta) = -\frac{\overline{u_1' u_2'}}{u_\tau^2}. \tag{B 20}$$

Using equation (B 14) to rewrite the right-hand side of equation (B 1) gives, together with equations (B 3), (B 15), (B 16) and (B 20) a momentum equation of the following form:

$$\frac{1}{H_{12}}g'(\eta) = \eta F'(\eta) + \gamma\left\{\frac{1}{\varkappa}(\eta F(\eta))' - F'(\eta)\left(\int_{\eta_0}^{\eta} F(\xi)\mathrm{d}\xi + \eta_0 F(\eta_0) + \frac{\eta_0}{\varkappa}\right)\right\} + O(\gamma^2). \tag{B 21}$$

This equation can be solved in the region where the exponential velocity defect law, (1.15), was found to agree well with experimental data.

We may express the Reynolds shear stress as a series expansion in γ,

$$g(\eta) = g_0(\eta) + \gamma g_1(\eta) + O(\gamma^2). \tag{B 22}$$

To zeroth-order accuracy in γ we obtain

$$g_0'(\eta) = H_{12}\eta F'(\eta). \tag{B 23}$$

If $F(\eta)$ is taken here as the exponential velocity defect law, integration yields

$$g_0(\eta) - g_0(\eta_0) = H_{12}\frac{C_1}{C_2}\{(C_2\eta + 1)\exp(-C_2\eta) - (C_2\eta_0 + 1)\exp(-C_2\eta_0)\}. \tag{B 24}$$

For first order accuracy in γ we obtain, by combining equations (B 21) and (B 22), the following correction term to the Reynolds shear stress:

$$\begin{aligned} g_1(\eta) - g_1(\eta_0) = H_{12}\frac{C_1}{2C_2\varkappa}\{&2C_2(\eta - \eta_0)\exp(-C_2\eta) + C_1\varkappa\exp(-2C_2\eta) \\ &- 2C_1\varkappa(C_2\eta_0 + 1)\exp(-C_2(\eta + \eta_0)) + C_1\varkappa(2C_2\eta_0 + 1)\exp(-2C_2\eta_0)\}. \end{aligned} \tag{B 25}$$

The complete expression for the normalized shear stress, to first-order accuracy in γ, is found by introducing (B 24) and (B 25) into equation (B 22). One could also consider an order-γ correction to the exponential velocity defect law. By studying the magnitude of the terms of order γ included in the approximation (B 21) one can conclude, however, that the $O(\gamma)$-correction to $F(\eta)$ must give a negligible contribution for the Reynolds number variation observed in figure 5. This is also evidenced by the fact that the solution $g_0(\eta) + \gamma g_1(\eta)$ accurately approximates the measured Reynolds shear stress (see figure 11).

REFERENCES

Afzal, N. & Yajnik, J. 1973 Analysis of turbulent pipe and channel flows at moderately large Reynolds number. *J. Fluid Mech.* **61**, 23–31.

Barenblatt, G. I. 1993 Scaling laws for fully developed turbulent shear flows. Part 1. Basic hypotheses and analysis. *J. Fluid Mech.* **248**, 513–520.

Blackwelder, R. F. & Kaplan, R. E. 1976 On the wall structure of the turbulent boundary layer. *J. Fluid Mech.* **76**, 89–112.

Buschmann, M. H. & Gad-el-Hak, M. 2002 Reynolds-number-dependent scaling law for turbulent boundary layers. In *IUTAM Symp. on Reynolds Number Scaling in Turbulent Flow*. Princeton University, NJ, USA.

Cantwell, B. J. 2002 *Introduction to Symmetry Analysis*. Cambridge University Press.

Coles, D. E. 1956 The law of the wake in the turbulent boundary layer. *J. Fluid Mech.* **1**, 191–226.

George, W. K. & Castillo, L. 1997 Zero-pressure-gradient turbulent boundary layer. *Appl. Mech. Rev.* **50**, 689–729.

Hydon, P. 2000 *Symmetry Methods for Differential Equations – A Beginner's Guide*. Cambridge University Press.

von Kármán, T. 1930 Mechanische Aehnlichkeit und Turbulenz. *Nachr. Ges. Wiss. Göttingen, Math. Phys. Kl.* pp. 58–68 (also NACA TM 611).

Lewkowicz, A. K. 1982 An improved universal wake function for turbulent boundary layers and some of its consequences. *Z. Flugwiss. Weltraumforsch* **9** (Heft 4), 513–520.

Millikan, C. B. 1938 A critical discussion of turbulent flows in channels and circular tubes. In *Proc. Fifth Intl Congress of Applied Mechanics*, pp. 386–392. Wiley.

Moser, R. D., Kim, J. & Mansour, N. N. 1999 Direct numerical simulation of turbulent channel flow up to $Re_\theta = 590$. *Phys. Fluids* **11**, 943–945.

Oberlack, M. 1999 Similarity in non-rotating and rotating turbulent pipe flows. *J. Fluid Mech.* **379**, 1–22.

Oberlack, M. 2000 On symmetries on invarient solutions of laminar and turbulent wall-bounded flows. *Z. Angew. Math. Mech.* **80** (11–12), 791–800.

Oberlack, M. 2002 Symmetries and invariant solutions of turbulent flows and their implications for turbulence modelling. In *Theories of Turbulence* (ed. M. Oberlack & F. H. Busse). CISM International Centre for Mechanical Sciences Series. Springer.

Oberlack, M. 2001 A unified approach for symmetries in plane parallel turbulent shear flows. *J. Fluid Mech.* **427**, 299–328.

Oberlack, M. & Peters, N. 1993 Closure of the two-point correlation as a basis of Reynolds stress models. In *Near Wall Turbulent Flows* (ed. R. So, C. Speziale & B. Launder) pp. 85–94. Elsevier.

Österlund, J. M. 1999 Experimental studies of zero pressure-gradient turbulent boundary-layer flow. PhD thesis, Department of Mechanics, Royal Institute of Technology, Stockholm.

Österlund, J. M., Johansson, A. V. & Nagib, H. M. 2000*a* Comment on 'a note on the intermediate region in turbulent boundary layers' [Phys. Fluids 12, 2159]. *Phys. Fluids* **12**, 2360–2363.

Österlund, J. M., Johansson, A. V., Nagib, H. M. & Hites, M. H. 2000*b* A note on the overlap region in turbulent boundary layers. *Phys. Fluids* **12**, 1–4.

Perry, A. E., Hafez, S. & Chong, M. S. 2001 A possible reinterpretation of the Princeton superpipe data. *J. Fluid Mech.* **439**, 395–401.

Perry, A. E., Marušić, I. & Li, J. D. 1994 Wall turbulence closure based on classical similarity laws and the attached eddy hypothesis. *Phys. Fluids* **6**, 1024–1035.

Schultz-Grunow, F. 1940 Neues Reibungswiederstandsgesetz für glatte Platten. *Tech. Rep.* 8. Luftfahrtforschung (translated as New frictional resistance law for smooth plates, *NACA TM*-986, 1941).

Skote, M. 2001 Studies of turbulent boundary layer flow through direct numerical simulation. PhD thesis, Department of Mechanics, Royal Institute of Technology, Stockholm.

Smith, D. & Walker, J. 1959 Skin-friction measurements in incompressible flow. *NASA TR* R-26.

Wosnik, M., Castillo, L. & George, W. K. 2000 A theory for pipe and channel flows. *J. Fluid Mech.* **421**, 115–145.

Zagarola, M. V., Perry, A. E. & Smits, A. J. 1997 Log laws or power laws: The scaling in the overlap region. *Phys. Fluids* **9**, 2094–2100.